Int. J. Electrochem. Sci., 10 **(2015)** 10554 - 10564

International Journal of
ELECTROCHEMICAL
SCIENCE
www.electrochemsci.org

Synthesis and Electrocatalytic Performance of Co_3O_4 Modified Mn_3O_4 Composites in Zinc-Air Batteries

Guanghua Li, Ke Zhang, Mohammed Adnan Mezaal, Lixu Lei[*]

School of Chemistry and Chemical Engineering, Southeast University, Nanjing 211189, China
[*]E-mail: lixu.lei@seu.edu.cn

Received: 28 July 2015 / *Accepted:* 31 August 2015 / *Published:* 4 November 2015

Herein, we report a Co_3O_4 modified Mn_3O_4 composites. The samples were synthesized by the citrate method. The results show that the optimal composite is of the Co/Mn atomic ratio of 1:9. At current density of 226 mA cm^{-2}, the $Mn_{2.7}Co_{0.3}O_4$ sample shows the maximum power density of ~139 mW cm^{-2}. The sample $Mn_{0.90}Co_{0.10}$ displays a relatively low charge potential (~2.12 V) and high discharge potential (~1.12 V) with lower overpotential (~1.00 V), which strongly indicates good cycling ability of the rechargeable zinc-air battery as well as to the outstanding ORR and OER activities in alkaline medium.

Keywords: Zinc-air batteries; ORR; OER; Bifunctional catalyst

1. INTRODUCTION

With rising price of fossil fuels and its limited nature, the need for advanced energy conversion and storage devices have never been higher [1]. Metal-air, such as zinc-air batteries, is promising candidate for the next generation energy storage device, which have extremely high theoretical specific energy density for applications such as electric vehicles (EVs) [2]. However, the performance of a primary zinc-air battery is limited largely by the high cost and low catalytic performance of materials used. Furthermore, the limitation rechargeable zinc-air battery is due to the fact that the overpotentials of ORR and OER on the air electrode are generally high [3]. These high overpotentials decrease the efficiencies for discharging and charging reactions [4].

At present, the extensively used ORR and OER catalysts are still Pt [5], Ir [6] and its alloys [7-10] due to their relatively high activity and stability, but the scarcity of them hampers the large-scale applications of these clean energy technologies [4]. Transition metal oxides, such as Mn/Mn-based oxides [11-17] and Co/Co-based oxides [18-25] were developed to achieve the purpose of low costly,

highly active electrocatalysts for the ORR and OER [26, 27]. The mean electron transfer number of α-MnO_2/XC72 composite is ~3.95, revealing an excellent electrocatalyst toward ORR [11]. Electrochemical investigations show that the synthesized Mn_2O_3, which display remarkable electrocatalytic performance (comparable to commercial Pt/C catalyst) toward ORR in alkaline condition [28]. The α-MnO_2 displays superior ORR performance compared to birnessite-type MnO_2 [29]. The electrochemical properties of α-manganese oxide were researched toward ORR in both aqueous and organic electrolytes [14]. The Co-N-MWNTs display substantially improved property compared to Pt/C catalyst toward ORR in Li-O_2 batteries [30]. Co_3O_4/Co_2MnO_4 nanocomposite shows superior bifunctional electrocatalytic properties toward ORR and OER, which can be attributed to the large specific surface area and well-dispersed heterogeneous structure of nanocomposite [22].

Hence, we expect that the combination of Mn_3O_4 and Co_3O_4 can enhance electrocatalytic property about ORR and OER. This paper, we demonstrate the Mn_3O_4 modified Co_3O_4 hybrid material and study their use in rechargeable ZABs.

2. EXPERIMENTAL

2.1 Synthesis of Co_3O_4/Mn_3O_4 hybrid materials

Co_3O_4 modified Mn_3O_4 hybrid material was synthesized by the citrate method [31]. $Mn(NO_3)_2{\cdot}4H_2O$, $Co(NO_3)_2{\cdot}6H_2O$ and citric acid were used as raw materials. The concentration of $Mn(NO_3)_2{\cdot}4H_2O$ was changed according to the Co/Mn atomic ratio of 2:3, 3:7, 1:4 and 1:9.

2.2 Materials characterization

The sample morphology was observed with a SEM (Hitachi S-4800), which was attached to an EDS. Powder diffraction was carried out with an XRD (Bruker D8 GADDS). Co and Mn contents were determined using an ICP (Optima 8000). Thermogravimetric (TG) measurements were measured by a TA-SDTQ600 thermal analyzer.

2.3 Manufacture of air electrode

The air electrodes were prepared in the same method that we reported earlier [32]. In brief, a mixture of $Mn_{3-3x}Co_{3x}O_4$ (x = 0 ~ 0.4) catalyst and acetylene black was grinded for 30 min, then the mixture and PTFE suspension (60 wt% in H_2O) with weight ratios of 8:2 were mixed and ground and then dried at 70 °C to give a dough-like paste, which was finally rolled into an Ni-mesh.

2.4 Electrochemical analysis

The polarization curves were performed with a half-cell using an electrochemical workstation system (CorrTest CS350). The electrolyte was 7 M KOH aqueous solution. The cathode was used as

the working electrode, while a nickel sheet and an Hg/HgO electrode were used as counter electrode and a reference electrode, respectively.

2.5 Zinc-air cell manufacture and testing

A home-made zinc-air cell device was designed about the battery test. The electrolyte was 7 M KOH, and a zinc plate was used as the anode. ZABs testing were carried out at room temperature using a multichannel battery cycling unit (SZLAND CT2001C).

3. RESULTS AND DISCUSSION

3.1 Characterization of Co_3O_4/Mn_3O_4 hybrid materials

To understand the decomposition behaviors of $Mn_{3-3x}Co_{3x}O_4$ (x = 0 ~ 0.4) precursor, the TG curves of $Mn_{2.4}Co_{0.6}O_4$ precursor is given in Fig. 1. Fig.1 shows that the TGA curve contains two processes of weight loss. The first process between 50 and 200 °C displays a small weight loss, which is attributed to a removal of physical adsorbed water in the material. The second process between 200 and 500 °C reveals a decrease with large weight loss of 58.3% which can be attributed to the decomposition of the oxynitride ions as well as carbon dioxide. Beyond 500 °C, there is no weight loss could be observed. It indicates that the cobalt/manganese citrate were overall converted to relevant Co_3O_4/Mn_3O_4.

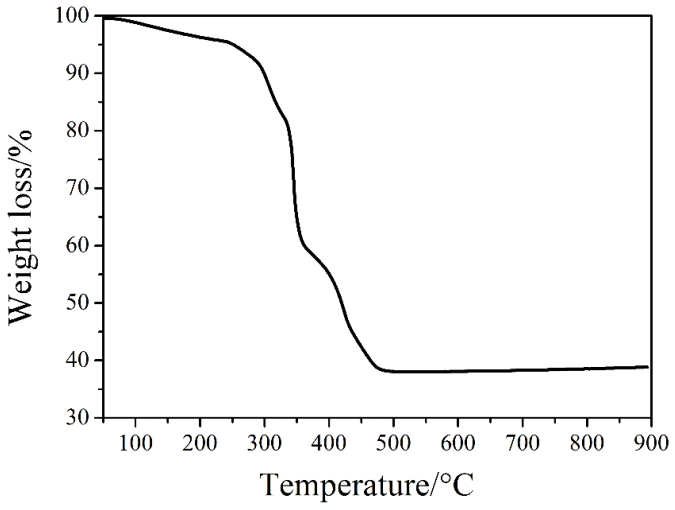

Figure 1. TGA curves of the $Mn_{2.4}Co_{0.6}O_4$ precursor.

Fig. 2 shows XRD patterns of Co_3O_4 modified Mn_3O_4 samples with different Co/Mn atomic ratios. In comparison, the XRD pattern of Mn_3O_4 (JCPDS No. 24-734) is shown Fig. 2. It can be seen that the XRD patterns of the samples with the Co/Mn atomic ratio of 2:3, 3:7, 1:4 and 1:9 are

comparable and the main phases is Mn_3O_4, with the Co_3O_4 being the minor phase. The lattice parameters are listed in Table 1, which shows that both the values *a* and *c* increase as content of Co increases.

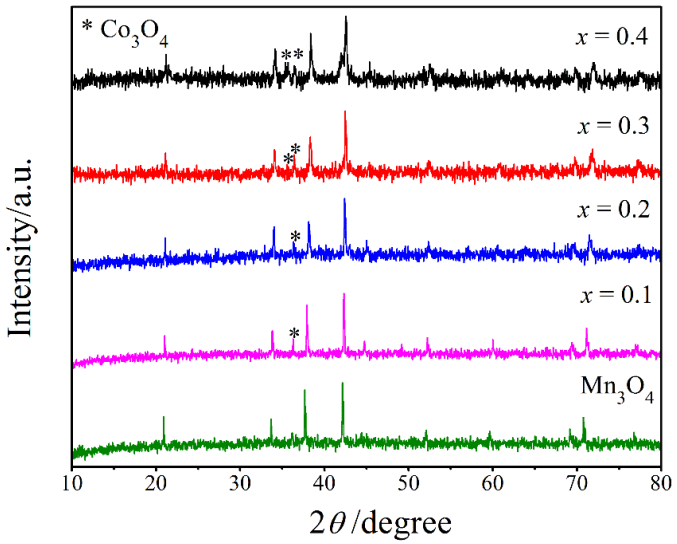

Figure 2. XRD patterns of $Mn_{3-3x}Co_{3x}O_4$(x = 0 ~ 0.4).

Table 1. The lattice parameters of $Mn_{3-3x}Co_{3x}O_4$ (x = 0 ~ 0.4).

Compose	$Mn_{1.8}Co_{1.2}O_4$	$Mn_{2.1}Co_{0.9}O_4$	$Mn_{2.4}Co_{0.6}O_4$	$Mn_{2.7}Co_{0.3}O_4$
a (Å)	5.7046	5.7065	5.7152	5.7317
c (Å)	9.2454	9.2764	9.3645	9.3837

The SEM images of the Co_3O_4 modified Mn_3O_4 composites with Co/Mn atomic ratio of 2:3 are shown in Fig. 3 (a), 3:7 (b), 1:4(c) and 1:9(d). The results show that the irregular morphologies of these samples at an aggregated form with an average diameter of 1 ~ 4 μm. In order to investigate the composition of the Co_3O_4/Mn_3O_4, EDS analysis were also performed in Fig.3. The EDS results revealed the existence of cobalt and manganese with different proportions (Table 2).

Table 2. Atom % of $Mn_{3-3x}Co_{3x}O_4$(x = 0 ~ 0.4) for EDS.

Atom %	O-K	Mn-K	Co-K
$Mn_{1.8}Co_{1.2}O_4$	57.33	25.75	16.92
$Mn_{2.1}Co_{0.9}O_4$	58.43	29.13	12.44
$Mn_{2.4}Co_{0.6}O_4$	57.23	34.29	8.48
$Mn_{2.7}Co_{0.3}O_4$	56.89	38.77	4.34
Mn_3O_4	42.83	57.17	—

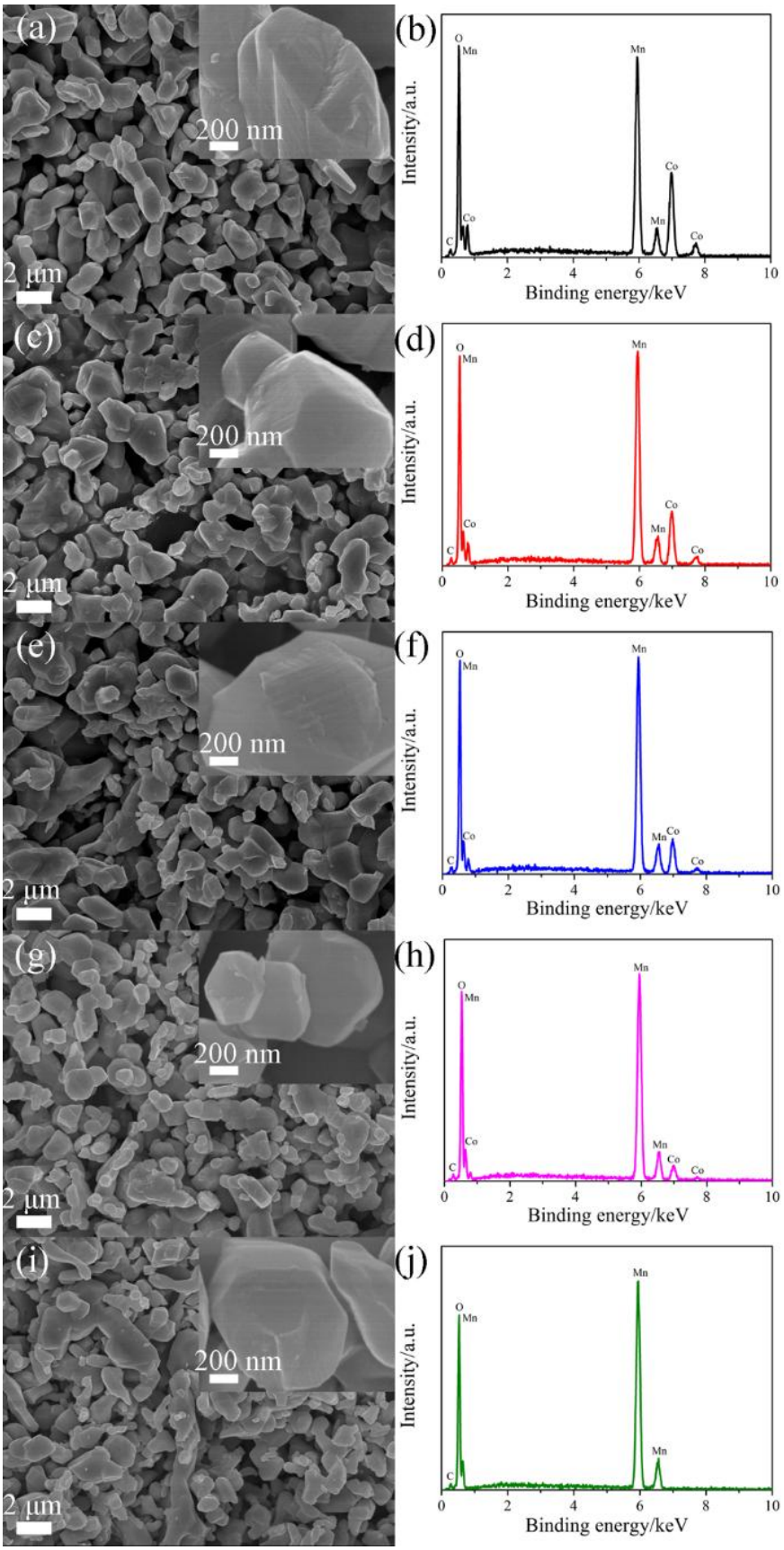

Figure 3. SEM images and EDS spectra of $Mn_{1.8}Co_{1.2}O_4$ (a, b), $Mn_{2.1}Co_{0.9}O_4$ (c, d), $Mn_{2.4}Co_{0.6}O_4$ (e, f), $Mn_{2.7}Co_{0.3}O_4$ (g, h) and Mn_3O_4 (i, j).

Co and Mn composition of the materials were performed by ICP. Herein, according to the different weight ratios $Mn_{3-3x}Co_{3x}O_4$(x = 0 ~ 0.4). The analytical results are shown in Table 3. It is found that the chemical compositions of the synthesized samples are $Mn_{1.83}Co_{1.17}O_4$, $Mn_{2.13}Co_{0.87}O_4$, $Mn_{2.43}Co_{0.57}O_4$, $Mn_{2.70}Co_{0.30}O_4$ and Mn_3O_4. This results are very close to the proposed $Mn_{1.8}Co_{1.2}O_4$, $Mn_{2.1}Co_{0.9}O_4$, $Mn_{2.4}Co_{0.6}O_4$, $Mn_{2.7}Co_{0.3}O_4$ and Mn_3O_4 chemical stoichiometry.

Table 3. Element content of the $Mn_{3-3x}Co_{3x}O_4$(x = 0 ~ 0.4).

Sample		Co (mg/g)	Mn (mg/g)
Proposed	Found		
$Mn_{1.8}Co_{1.2}O_4$	$Mn_{1.83}Co_{1.17}O_4$	303 (295)	423 (431)
$Mn_{2.1}Co_{0.9}O_4$	$Mn_{2.13}Co_{0.87}O_4$	228 (221)	496 (504)
$Mn_{2.4}Co_{0.6}O_4$	$Mn_{2.43}Co_{0.57}O_4$	153 (145)	570 (578)
$Mn_{2.7}Co_{0.3}O_4$	$Mn_{2.70}Co_{0.30}O_4$	76.9 (76.9)	645 (645)
Mn_3O_4	Mn_3O_4	—	720 (720)

* Values are found (calculated according to the found compositions).

3.2 Electrocatalytic ORR and OER

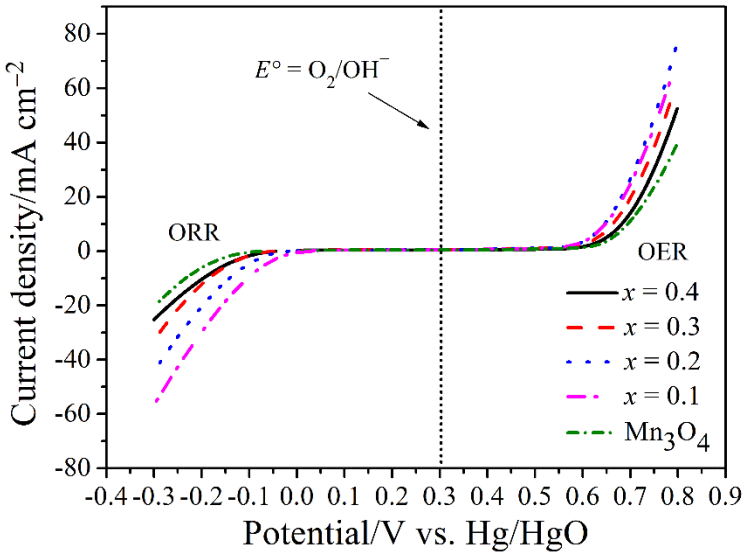

Figure 4. The cathode and the anode polarization curves of $Mn_{3-3x}Co_{3x}O_4$ (x = 0 ~ 0.4).

The activity of the Mn_3O_4 and Co_3O_4/Mn_3O_4 hybrid materials for ORR and OER in an aqueous alkaline solution was evaluated by polarization curves are shown in Fig. 4. At a cathodic current density of 10 mA cm^{-2}, the $Mn_{2.7}Co_{0.3}O_4$ operated at ~93 mV more positive potential than $Mn_{1.8}Co_{1.2}O_4$, ~81 mV more positive potential than $Mn_{2.1}Co_{0.9}O_4$, ~38 mV more positive potential than $Mn_{2.4}Co_{0.6}O_4$, and ~130 mV more positive potential than Mn_3O_4, showed the highest ORR catalytic

activity. At an anodic current density of 10 mA cm^{-2}, the polarization of the $Mn_{2.4}Co_{0.6}O_4$ was ~37 mV more negative than $Mn_{1.8}Co_{1.2}O_4$, ~18 mV more negative than $Mn_{2.1}Co_{0.9}O_4$, ~3 mV more negative than $Mn_{2.7}Co_{0.3}O_4$, and ~49 mV more negative than Mn_3O_4, was active for OER. The bifunctional catalytic activity was calculated by the sum of ORR and OER overpotentials. The overpotentials (ΔE) of $Mn_{1.8}Co_{1.2}O_4$, $Mn_{2.1}Co_{0.9}O_4$, $Mn_{2.4}Co_{0.6}O_4$, $Mn_{2.7}Co_{0.3}O_4$ and Mn_3O_4 are found to be 879, 848, 787, 752 and 928 mV. Simultaneously, the $Mn_{2.7}Co_{0.3}O_4$ exhibits highest catalytic activity for ORR and OER. The cathodic and anodic overpotential of $La_{0.9}Ca_{0.1}CoO_3$ was 246 and 648 mV, respectively [33].

3.3 Primary zinc-air batteries

Fig. 5 shows the polarization and power density curves of the zinc-air batteries with the $Mn_{1.8}Co_{1.2}O_4$, $Mn_{2.1}Co_{0.9}O_4$, $Mn_{2.4}Co_{0.6}O_4$, $Mn_{2.7}Co_{0.3}O_4$ and Mn_3O_4 catalysts. At 1.0 V, $Mn_{1.8}Co_{1.2}O_4$, $Mn_{2.1}Co_{0.9}O_4$, $Mn_{2.4}Co_{0.6}O_4$, $Mn_{2.7}Co_{0.3}O_4$ and Mn_3O_4 afforded an ORR current density of ~70, ~71, ~77, ~85 and ~66 mA cm^{-2}, respectively. The results indicate that the $Mn_{2.7}Co_{0.3}O_4$ is more active than $Mn_{1.8}Co_{1.2}O_4$, $Mn_{2.1}Co_{0.9}O_4$, $Mn_{2.4}Co_{0.6}O_4$, and Mn_3O_4 for ORR activity. At current density of 226 mA cm^{-2}, The maximum power density achieved by zinc-air cell using $Mn_{2.7}Co_{0.3}O_4$ catalyst was ~139 mW cm^{-2} which is about 15%, 13%, 5% and 24% higher than that of zinc-air cell using $Mn_{1.8}Co_{1.2}O_4$ (~120 mW cm^{-2} at 206 mA cm^{-2}), $Mn_{2.1}Co_{0.9}O_4$ (~123 mW cm^{-2} at 207 mA cm^{-2}), $Mn_{2.4}Co_{0.6}O_4$ (~132 mW cm^{-2} at 224 mA cm^{-2}), and Mn_3O_4 (~112 mW cm^{-2} at 185 mA cm^{-2}), respectively. The peak power density XC72/α-MnO_2 is 67.51 mW cm^{-2} [11]. It was reported that the peak power density of Ni modified MnO*x* composite reached 122 mW cm^{-2} [12].

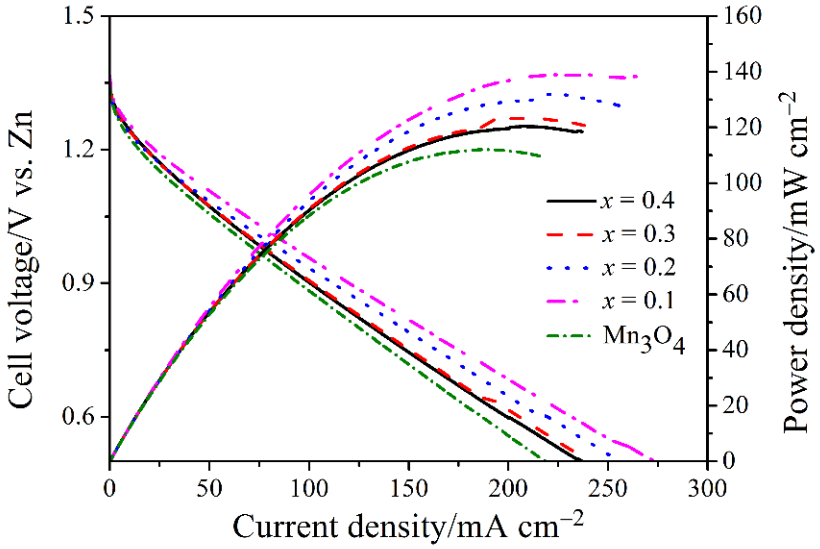

Figure 5. Polarization and power density curves of $Mn_{3-3x}Co_{3x}O_4$ (x = 0 ~ 0.4).

Fig. 6 shows the typical discharge profiles of home-made primary zinc-air cells made with $Mn_{1.8}Co_{1.2}O_4$, $Mn_{2.1}Co_{0.9}O_4$, $Mn_{2.4}Co_{0.6}O_4$, $Mn_{2.7}Co_{0.3}O_4$ and Mn_3O_4. At a constant current density of 30 mA cm^{-2} for the cells with the catalysts, the working voltage plateaus were ~1.09, ~1.06, ~1.10, ~1.07 and ~1.03 V; discharge lasted for 20.5 h, 22.7 h, 22.6 h, 24.6 h and 20.6 h, respectively. While, at a constant current density of 50 mA cm^{-2} for the cells with the catalysts, the working voltage plateaus were ~1.04, ~0.93, ~1.00, ~1.01 and ~0.94 V; discharge lasted for 10.7 h, 12.8 h, 12.8 h, 14.2 h and 12.6 h, respectively. The zinc-air cell voltage of XC72/α-MnO_2 is equal to 1.35 and 1.17 V at 2 and 20 mA cm^{-2}, respectively. Furthermore, it can sustain ~11.5 h at 10 mA cm^{-2} with its discharge plateaus of 1.2 V [11]. The results indicate that the $Mn_{2.7}Co_{0.3}O_4$ ORR catalyst is preferably suited for such refueling primary zinc-air batteries owing to the exceptional ORR activity and durability.

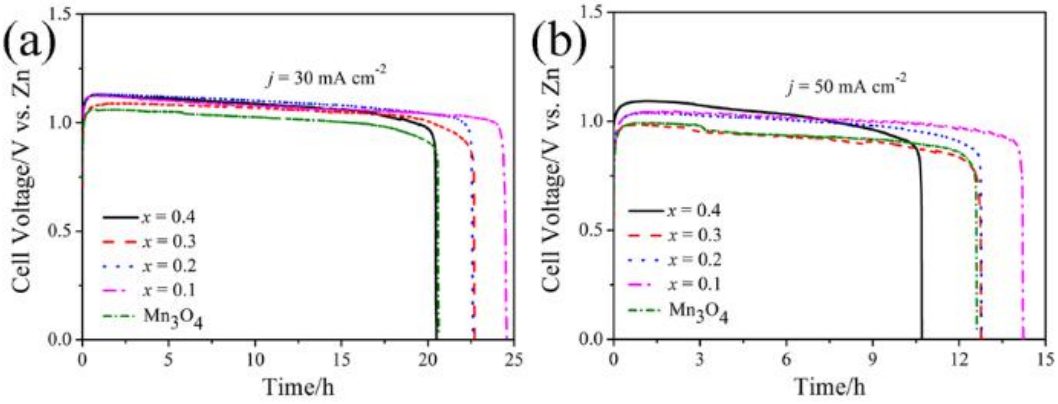

Figure 6. Discharge curves of zinc-air batteries with $Mn_{3-3x}Co_{3x}O_4$ (x = 0 ~ 0.4).

3.4 Rechargeable zinc-air batteries

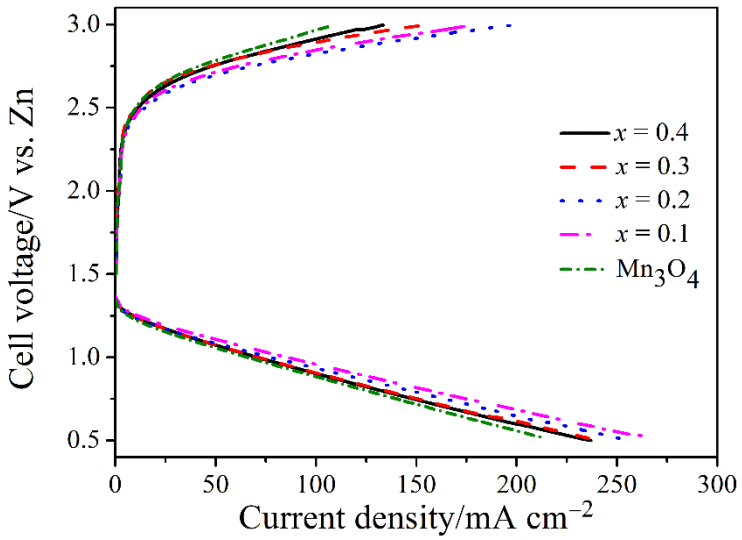

Figure 7. Charge and discharge polarization curves of the zinc-air battery using $Mn_{3-3x}Co_{3x}O_4$ (x = 0 ~ 0.4).

Fig. 7 shows the charge/discharge polarization profiles of a rechargeable zinc-air battery using $Mn_{1.8}Co_{1.2}O_4$, $Mn_{2.1}Co_{0.9}O_4$, $Mn_{2.4}Co_{0.6}O_4$, $Mn_{2.7}Co_{0.3}O_4$ and Mn_3O_4 catalyst loaded on Ni foam for ORR/OER electrode. The battery exhibits similar current densities as the rechargeable battery. The charge-discharge voltage gap at 10 mA cm^{-2} was 1.23, 1.25, 1.21, 1.20 and 1.27 V (voltage polarization contributed by the sum of OER and ORR overpotentials at the air electrodes [34]). Undoubtedly, the voltage gap of the battery with $Mn_{2.7}Co_{0.3}O_4$ catalyst is much smaller than $Mn_{1.8}Co_{1.2}O_4$, $Mn_{2.1}Co_{0.9}O_4$, $Mn_{2.4}Co_{0.6}O_4$, and Mn_3O_4. This test results suggest that high ORR-OER activity of $Mn_{2.7}Co_{0.3}O_4$ the actually function as an efficient bifunctional catalyst for ZABs.

Based on the promising half-cell performance, zinc-air battery implementing a zinc electrode was used to evaluate the $Mn_{3-3x}Co_{3x}O_4$ (x = 0 ~ 0.4) catalyst´s performance under realistic operating conditions. The stability of the $Mn_{3-3x}Co_{3x}O_4$ (x = 0 ~ 0.4) catalyst was examined via the charge-discharge cycling in 7 M KOH. We have used the same ORR and OER electrode for subsequent cycling experiment that was carried out by discharging and charging (10 min in each state) the battery at 10 mA cm^{-2} using the recurrent galvanic pulse method.

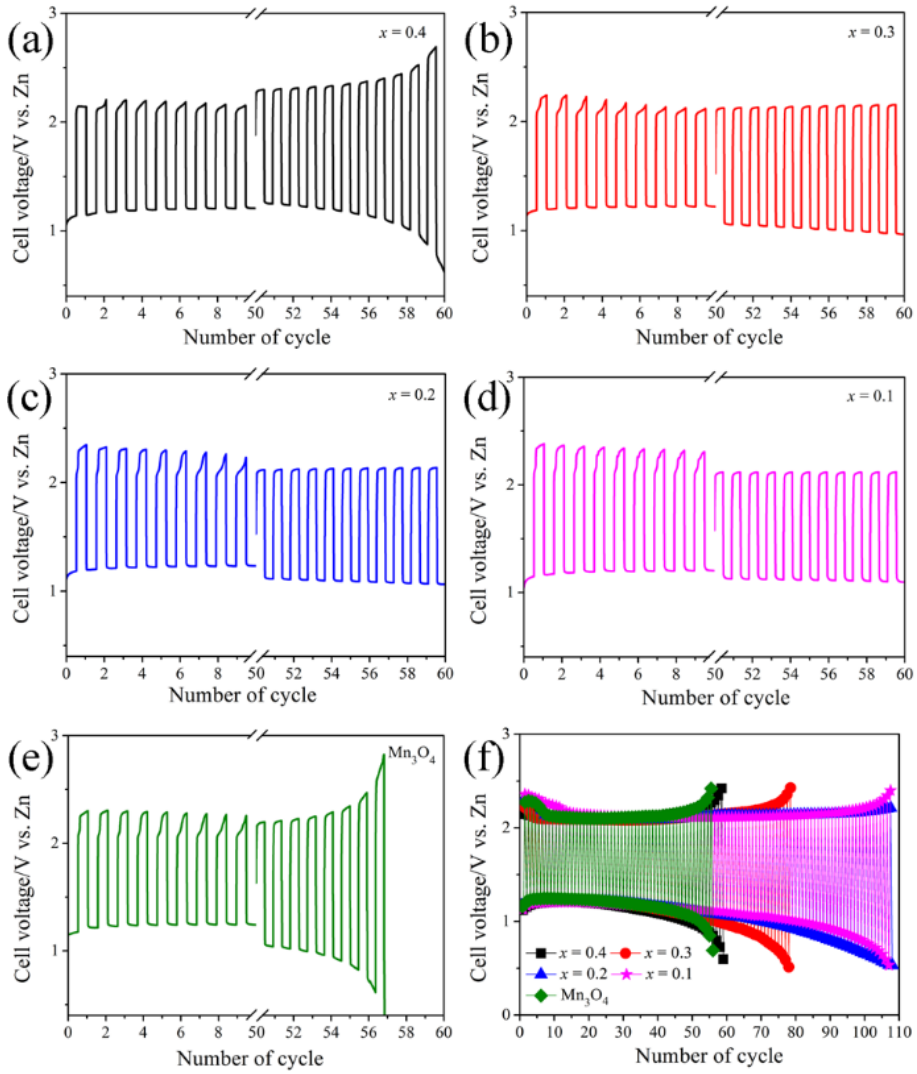

Figure 8. Charge-discharge cycling of the zinc-air battery with $Mn_{3-3x}Co_{3x}O_4$ (x = 0 ~ 0.4).

The first ten cycles display a similar discharge voltage and a lower charge plateau (see Fig. 8 for more information). After cycling the $Mn_{2.7}Co_{0.3}O_4$ electrode for 60 cycles, the final charge/discharge potential were ~2.12 and ~1.12 V, respectively, whereas the initial values were ~2.34 and ~1.20 V. The difference of voltage between the discharged and the initial for $Mn_{2.7}Co_{0.3}O_4$ after 60 cycles was ~1.14 V with overpotential of 0.14 V. The moderately low charge and high discharge potential with low overpotential that showed by $Mn_{2.7}Co_{0.3}O_4$ mean good recharge-ability of the ZABs as well as reasonable outstanding ORR/OER activities in alkaline condition. The $LaMnO_3$ ZABs shows a charge-discharge voltage gap of 1.63 V at ±25 mA cm^{-2} [35]. Our results showed a 5% and 20% change in the charge/discharge potentials for MnO_2-NCNT composite [27].

4. CONCLUSIONS

In summary, a new air electrode Co_3O_4/Mn_3O_4 hybrid materials were synthesized via a citrate method for primary and rechargeable zinc-air batteries. We construct primary zinc-air batteries using the $Mn_{2.7}Co_{0.3}O_4$ ORR catalyst for the air cathode, which delivers a high discharge current density of (226 mA cm^{-2}) with a peak power density of ~139 mW cm^{-2}. The $Mn_{2.7}Co_{0.3}O_4$ also exhibits good bifunctional ORR/OER activity and cycling stability in the charge/discharge process. The battery shows the smallest charge-discharge polarization of ~1.20 V and excellent cycling stability over repeated, 50 to 120 charge-discharge cycles at 10 mA cm^{-2}. Therefore, $Mn_{2.7}Co_{0.3}O_4$ catalyst is a very promising ORR/OER bifunctional electrocatalyst for ZABs.

ACKNOWLEDGMENTS
Jiangsu Province for the College graduate research and innovation projects (CXLX12_0105) is gratefully acknowledged for funding this work.

References

1. M. Winter, R.J. Brodd, *Chem. Rev.*, 104 (2004) 4245-4269.
2. Y. Li, H. Dai, *Chem. Soc. Rev.*, 43 (2014) 5257-5275.
3. M.K. Debe, *Nature* 486 (2012) 43-51.
4. G. Toussaint, P. Stevensa, L. Akroura, R. Rougetb, F. Fourgeotb, *ECS Transactions*, 28 (2010) 25-34.
5. J. Chen, B. Lim, E.P. Lee, Y. Xia, *Nano Today*, 4 (2009) 81-95.
6. Y. Zhao, E.A. Hernandez-Pagan, N.M. Vargas-Barbosa, J.L. Dysart, T.E. Mallouk, *J. Phys. Chem. Lett.*, 2 (2011) 402-406.
7. B.N. Wanjala, R. Loukrakpam, J. Luo, P.N. Njoki, D. Mott, C.J. Zhong, *J. Phys. Chem. C*, 114 (2010) 17580-17590.
8. B. Fang, B.N. Wanjala, J. Yin, R. Loukrakpam, J. Luo, X. Hu, J. Last, C.J. Zhong, *Int. J. Hydrogen Energ.*, 37 (2012) 4627-4632.
9. B. Fang, J. Luo, P.N. Njoki, R. Loukrakpam, D. Mott, B. Wanjala, X. Hu, C.J. Zhong, *Electrochem. Commun.*, 11 (2009) 1139-1141.

10. B. Lim, M. Jiang, P.H. Camargo, E.C. Cho, J. Tao, X. Lu, Y. Zhu, Y. Xia, *Science*, 324 (2009) 1302-1305.
11. P.C. Li, C.C. Hu, T.C. Lee, W.S. Chang, T.H. Wang, *J. Power Sources*, 269 (2014) 88-97.
12. Q. Wu, L. Jiang, L. Qi, E. Wang, G. Sun, *Int. J. Hydrogen Energ.*, 39 (2014) 3423-3432.
13. G. Du, X. Liu, Y. Zong, T.S. Hor, A. Yu, Z. Liu, *Nanoscale*, 5 (2013) 4657-4661.
14. E.M. Benbow, S.P. Kelly, L. Zhao, J.W. Reutenauer, S.L. Suib, *J. Phys. Chem. C*, 115 (2011) 22009-22017.
15. J.S. Lee, G.S. Park, H.I. Lee, S.T. Kim, R. Cao, M. Liu, J. Cho, *Nano Lett.*, 11 (2011) 5362-5366.
16. Y.J. Huang, Y.L. Lin, W.S. Li, *Electrochim. Acta*, 99 (2013) 161-165.
17. T.H. Yang, S. Venkatesan, C.H. Lien, J.L. Chang, J.M. Zen, *Electrochim. Acta*, 56 (2011) 6205-6210.
18. D.U. Lee, J. Scott, H.W. Park, S. Abureden, J.Y. Choi, Z. Chen, *Electrochem. Commun.*, 43 (2014) 109-112.
19. X.G. Fu, J.T. Jin, Y.R. Liu, Q. Liu, K.X. Niu, J.Y. Zhang, X.P. Cao, *Electrochem. Commun.*, 28 (2013) 5-8.
20. J. Xiao, Q. Kuang, S. Yang, F. Xiao, S. Wang, L. Guo, *Scientific Reports*, 3 (2013) 2300.
21. J. Wu, D. Zhang, Y. Wang, Y. Wan, B. Hou, *J. Power Sources*, 198 (2012) 122-126.
22. D. Wang, X. Chen, D.G. Evans, W. Yang, *Nanoscale*, 5 (2013) 5312-5315.
23. Y. Liang, Y. Li, H. Wang, J. Zhou, J. Wang, T. Regier, H. Dai, *Nat. Mater.*, 10 (2011) 780-786.
24. R. Huo, W.J. Jiang, S. Xu, F. Zhang, J.S. Hu, *Nanoscale*, 6 (2014) 203-206.
25. S. Zhuang, H. Zhang, S. Liu, F. Tu, W. Zhang, C. Zhao, *Int. J. Electrochem. Sci.*, 9 (2014) 1690-1701.
26. R. Cao, J.-S. Lee, M. Liu, J. Cho, *Adv. Energ. Mater.*, 2 (2012) 816-829.
27. Z. Chen, A. Yu, R. Ahmed, H. Wang, H. Li, Z. Chen, *Electrochim. Acta*, 69 (2012) 295-300.
28. F. Cheng, J. Shen, W. Ji, Z. Tao, J. Chen, *ACS Appl. Mater. Interf.*, 1 (2009) 460-466.
29. W. Xiao, D. Wang, X.W. Lou, *J. Phys. Chem. C*, 114 (2010) 1694-1700.
30. G. Wu, N.H. Mack, W. Gao, S. Ma, R. Zhong, J. Han, J.K. Baldwin, P. Zelenay, *ACS Nano*, 6 (2012) 9764-9776.
31. X. Wang, P.J. Sebastian, M.A. Smit, H. Yang, S.A. Gamboa, *J. Power Sources*, 124 (2003) 278-284.
32. G. Li, M.A. Mezaal, K. Zhang, L. Lei, *Int. J. Electrochem. Sci.*, 10 (2015) 5395-5404.
33. S.W. Eom, S.Y. Ahn, I.J. Kim, Y.K. Sun, H.S. Kim, *J. Electroceram.*, 23 (2008) 382-386.
34. Z. Chen, A. Yu, D. Higgins, H. Li, H. Wang, Z. Chen, *Nano Lett.*, 12 (2012) 1946-1952.
35. Y.C. Lee, P.Y. Peng, W.S. Chang, C.M. Huang, *J. Taiwan Inst. Chem. E.*, 45 (2014) 2334-2339.